Atmos. Meas. Tech. Discuss.,
doi:10.5194/amt-2020-202-AC1, 2020

Atmospheric Measurement Techniques Discussions

Interactive comment on "On the relationship between wind observation accuracy and the ascending node of sun-synchronous orbit for the Aeolus-type spaceborne Doppler wind lidar" *by* Chuanliang Zhang et al.

Chuanliang Zhang et al.

zhangcl2015@126.com

Received and published: 15 October 2020

Dear Dr. Gert-Jan Marseille,

We are truly grateful to your critical comments and thoughtful suggestions. Based on these comments and suggestions, we have made careful thoughts. We are now sending you the corresponding replies. Please point out the mistakes and weaknesses for correction if any. Below you will find our point-by-point responses to your comments/ questions, the comments and suggestions you gave are marked in blue, our replies are

marked in black. Please note that the last figure is Table 1 of the text:

1. The presented results are interesting and potentially useful input for discussions on an Aeolus follow-on mission. The main question, which has not been answered in the paper is: why selecting orbits other than dawn-dusk, given that 3 satellites in a dawn-dusk orbit gives already quite good global coverage, without reducing wind quality due to increased solar background? See Fig.4 of Marseille et al (2008). Is there some indication that different local overpass times would be favorable for NWP? Please elaborate on this in the paper.

Response: The main purpose of this manuscript is to access the impact of solar background radiation (SBR) on the accuracy of wind observations for spaceborne Doppler wind lidar (DWL). For spaceborne DWLs operate on sun-synchronous orbits, the dawn-dusk orbit will receive minimum SBR, and the noon orbit will receive maximum SBR. The spaceborne DWLs operate on the sun-synchronous orbits with local time of ascending node (LTAN) crossing of 15:00 will receive medium SBR.

Three spaceborne DWLs operate on a dawn-dusk orbit give quite good global coverage, however, they would receive similar SBR. To access the impact of orbits selection on the accuracy of wind observations, the three orbits with LTANs of 18:00, 15:00, and 12:00 were purposed. The influence of spaceborne DWLs operate on different orbits on NWP was not considered in this paper, because this is not the focus of this manuscript, but it is a very interesting topic that deserves further study.

2. In connection to this. Line 43: "The future spaceborne DWLs may operate on different orbits which should be related to their observation purposes". Which observation purposes are related to 12:00 or 15:00 local overpass times? See also line 72: "Assuming the future Aeolus-type spaceborne DWLs will operate on the sun-synchronous orbits with different LTAN". Based on what assumption?

Response: Apart from Aeolus, the hybrid Doppler wind lidar (HDWL) designed by US would utilize both direct-detection and coherent-detection technology to observe verti-

cal profile horizontal LOS (line-of-sight) wind vectors. SBR would lower the accuracy of wind observed by direct-detection technology. According to the National Polar-orbiting Operating Environmental Satellite System (NPOESS) mission, US would launch two HDWLs in two stages. Stage 1: Global Wind Observing Sounder (GWOS) mission: the mission aims to demonstrate the prototype HDWL system whether it would be capable of global wind measurements. GWOS would operate on a low earth orbit with orbit height of 400 km, the detailed parameters of the orbit are unknown. Stage 2: NPOESS Wind Observing Sounder (NWOS) mission: the mission would launch a HDWL system carried on the NPOESS satellites that would meet fully-operational wind measurement requirements. The NPOESS satellite constellation consists of 3 satellites in 828 km altitude, sun synchronous orbits, with LTANs of 13:30, 17:30, and 21:30. It is not clear which orbit the NWOS will operate. According to the stowed configuration of three satellites and the location of the NWOS shown in Figure 1 and 2, it is inferred that NWOS may operate on the orbit of 21:30.

This satellite orbits were designed in 15 year ago, and may be adjusted before the launch of satellites in the future. However, the fact illustrates that the future spaceborne DWL may operate not only on the sun synchronous dawn-dusk orbit. To some extent, the research in this manuscript will also provide references for the orbit selection of HDWL in NWOS.

On the other hand, supposed that one satellite constellation consists three spaceborne DWLs operate on sun synchronous orbits with LTANs of 18:00, 15:00, and 12:00, we can reconstruct the wind speed diurnal cycle according to the wind observations. For both wind observations and analyzed wind acquired from NWP shows the obvious diurnal characteristics of wind field: 1) the diurnal variations of wind speed follow cosine curve, approximately; 2) wind speed reaches its maximum value at about 23:00; 3) the analyzed wind speed has peak value during the sunrise (Zhang and Zheng, 2004, Holtslag et al., 2013).

3. The realism of the simulations can be largely improved by comparing Aeolus mea-

sured SBR with simulated Aeolus SBR. Information on Aeolus measured SBR and the impact on Aeolus wind quality is found in the attached supplementary material. Based on this information, the authors can test the realism of their simulations.

Response: The solar background noise (SBN) received by Aeolus is determined by the geometry of solar and satellite, atmospheric conditions, and earth reflectance. And the solar zenith angle (SZA) of the off-nadir points is the main determinants. The simulated SZAs of the off-nadir points within one-year range are shown in Fig. 3. When the solar zenith angle is greater than 90 degrees as the horizontal red line shows, the received SBR could be negligible. Comparisons between Fig. 3 and Fig. 1 of the supplement provided by reviewer 1 show high consistence. Both of them are periodic. The values of them reach maximum near summer solstice and reach maximal near winter solstice. And the values of SBR reach minimal values near spring and autumn equinox. The 4 time ranges in Fig. 3 divided by 8 red lines denote 15 days near autumn equinox, winter solstice, spring equinox, summer solstice.

It requires great amount of computing to simulate the received SBR of Aeolus with one-year range. The received SBR within 15 days near summer and winter solstice was simulated. And the SBR in summer and winter solstice was converted to ACCD counts of Rayleigh channel as is illustrated in Fig. 4.

As Fig. 4 illustrated, the amount of ACCD counts near summer and winter solstice are consistent with Fig. 1 of the supplement. And solar background noise excited on Rayleigh channel are periodic as the subgraph of the supplement shows.

In order to facilitate reviewers to verify the simulation model of Aeolus used in this manuscript, we would introduce the method and the parameters used in this manuscript which are mainly derived from ATBD ADM-Aeolus Level1B Products (issue 3.0, 30.11.2006) (Reitebuch et al., 2006). The energy of solar background noise denotes in photon counts before Rayleigh channel can be expressed as

$$n_{solar} = n_{meas} \cdot n_{pulse} \cdot C(\lambda) \cdot L_{\lambda}(\Theta, \psi, \lambda) \cdot \Omega_0 \cdot A_0 \cdot t_D \cdot \Delta\lambda \cdot \lambda / (h \cdot c), \qquad (1)$$

where n_{meas} is the number of measurements in one observation. n_{pulse} is the number of pulses in one measurement. $C(\lambda)$ denote the transmission of optical instrument of ALADIN. $L_\lambda(\Theta, \psi, \lambda)$ denote the solar background radiation. Ω_0 denote the acceptance solid angle. A_0 is the area of telescope. t_D is the detection time for the solar background range gate. $\Delta\lambda$ is the bandwidth of the receiver. λ denote the wavelength of the laser. And h denote Plank constant, c denote the light speed.

The energy excited by SBN before the Rayleigh channel can be computed using Eq. (1). Assuming that the spectrum of SBN follows uniform distribution, and the energy is equal to the result of Eq. (1), its bandwidth equal to the Free Spectral Range of Rayleigh channel, the photon counts excited on Rayleigh channel can be obtained after transmitting through the Fabry-Perot interferometer and multiplying by the quantum efficiency of ACCD.

According to the latest issue of Aeolus ATBD L1B Products (Reitebuch et al., 2018), the latest parameters of ALADIN is different from the parameters we used in the manuscript, as is mentioned by reviewer 2. The comparisons of the parameters are illustrated in Table 1 as the last figure shows at the end of the text.

The simulated SBN using old parameters is shown in Fig. 5. The comparison between Fig. 4 and 5 illustrated that larger energy is excited using old parameters. More laser pulses are accumulated in one observation and the wider bandwidth of the FWHM and Free Spectral Range of FP interferometer in old parameters can account for this phenomenon.

Then, under the same atmospheric conditions, how much difference will the wind observations uncertainties obtained by using the new and old parameters be? The simulated uncertainties of wind observations under cloud-free atmospheric condition are illustrated in Fig. 6. The corresponding solar zenith angle of Fig. 6 is 70°, and the related solar background radiation is 72.19 mW$\cdot m^{-2}\cdot sr^{-1}\cdot nm^{-1}$. As Fig. 6 (a) shows, the difference of uncertainties simulated using old and new parameters is large. The

largest and average difference is 2.17 and 0.61 m/s, respectively. Fig. 6 (b) illustrated that the SNR simulated using new parameters is obviously large than the results using old parameters. The combination of Figs. 6 (c, d) can account this phenomenon. In Fig. 6 (c), the simulated useful signal of Rayleigh channel is relatively close, almost no difference. However, Fig. 6 (d) illustrated that the simulated solar background noise obtained using old parameters is much large than that of new parameters. Why the solar background noise simulated using old parameters is much larger than that of new parameters? As Tab. 1 illustrated, under old parameters, the Free Spectral Range of Rayleigh channel and FWHM of the FP interferometers of the old parameters is much larger than that of the new parameters. And in the simulation process, the SBN is regarded as following uniform distribution. Wider transmission bandwidth of Rayleigh channel will lead to higher solar background energy, which would lower the SNR of Rayleigh channel, and then increase the uncertainties of wind observations.

To verify the correctness of our simulation model, we reconstructed Fig. 2 of the supplement using new parameters of Tab. 1 and the results are shown in Fig. 7. In the simulation, the typical and worst solar background radiation are set as 72.50 and 156.00 mW$\cdot m^{-2}\cdot sr^{-1}\cdot nm^{-1}$. The comparisons between Fig. 7 and Fig. 2 of the supplement show large difference. In Fig. 2 of the supplement, when the useful signal in channel A reach 5000, the related wind observation uncertainty is about 4 m/s. In our simulation, the uncertainty is about 8 m/s when the useful signal in channel A is about 5000. However, the uncertainties of wind observation are about 2$\sim$3 m/s when the solar background radiation is about 72.19 mW$\cdot m^{-2}\cdot sr^{-1}\cdot nm^{-1}$. The results are reasonable. In our simulation, the photon counts excited by typical and worst solar background noise in channel A are 1.34*10^4 and 2.92*10^4 respectively when the vertical height of the range gate is 1 km. In Fig. 6, the useful signal in channel A is general between 2*10^4 $\sim$ 3*10^4. I suppose the cause for this phenomenon maybe different instrument parameters used in our simulation or the polarization effects may not considered in our simulation, which lead to lager simulation results of the SBN and useful signal of channel A. The Matlab script used to simulate the results of Fig. 7 are

attached in the supplement for further discussion. Please point out and give directions to us whenever you see any weaknesses or shortages within.

==========Minor comments ==========

4. line 60: "The received SBR of Aeolus ranges from 0 to 169 mW·m-2·sr-1·nm-1". That is worse than "On the two new orbits, the increments of averaged SBR received by the new spaceborne DWLs range from 39 to 56 mW·m-2·sr-1·nm-1" (line 14). Can the author please comment.

Response: Line 14: "On the two new orbits, the increments of averaged SBR received by the new spaceborne DWLs range from 39 to 56 mW·m^{-2}·sr^{-1}·nm^{-1}." The sentence is referred to that the averaged SBR received by Aeolus-type instruments operate on the sun-synchronous orbits with LTANs of 15:00 and 12:00 is higher than Aeolus, and the average increment of SBR ranges from 39 to 56 mW·m^{-2}·sr^{-1}·nm^{-1}. The conclusion is corresponding to the sentence: "Statistics illustrate that the averaged SBR of the three spaceborne DWLs are 20.99, 60.68, and 76.36 mW·m^{-2}·sr^{-1}·nm^{-1} respectively." (line 262).

The sentence in line 14 may be ambiguous. In the revision, line 262 will be modified to make the sentence in line more clear as reviewer 2 suggest.

Modified: Statistics illustrate that the averaged SBR of the three spaceborne DWLs are 20.99, 60.68, and 76.36 mW·m^{-2}·sr^{-1}·nm^{-1} respectively. The increments of averaged SBR received by the new spaceborne DWLs are 60.68-20.99=39.69 mW·m^{-2}·sr^{-1}·nm^{-1} and 76.36-20.99=55.37 mW·m^{-2}·sr^{-1}·nm^{-1}.

5. Figure 1b is misleading since it suggests that all three Aeolus-type instruments operate during daytime at equal time intervals.

Response: Figure 1b illustrates the off-nadir points on earth surface of the three spaceborne DWLs operate on the sun-synchronous orbits with LTANs of 18:00, 15:00, and 12:00, respectively.

6. line 108: "Figure 1(b) shows that the solar zenith angle of the observation points of the two new Aeolus-type instruments is low compared to that of Aeolus". How can that be seen from the figure?

Response: In Figure 1 (b), the shaded area represents the night, the non-shaded area represents the day, and the dividing line between the shaded area and the non-shaded area is the dividing line between day and night. In Figure 1b, the trajectory of the off-nadir points of Aeolus is closer to the dividing line compared to the off-nadir points of Aeolus2 and Aeolus3. Therefore, it is supposed that the solar zenith angles of the off-nadir points of the two new orbits should be lower.

As the referee pointed, it is not clear to see the comparative relationship in the sun zenith angle of the three orbits. In the latter revision, we plan to add a figure to illustrate the fact in the revision, as Fig. 8 shows, which illustrate the variations of solar zenith angle of the three orbits as time.

7. The simulations would be more useful if the operational Aeolus instrument would be used for reference 1. one measurement is composed of 20 accumulated shots onboard; 1 observation is obtained from averaging 30 measurements. 2. Assuming around 60mJ laser energy, which is consistent with current operational Aeolus laser-B 3. optical throughput is a factor 2-3 lower than expected. The authors can do simulations based on both this unexpected signal loss (worst case scenario) and without this loss, assuming that the problem can be identified and solved before the launch of the Aeolus follow-on mission (best case scenario). With the above settings 0% of Aeolus data would meet the mission requirement, rather than 88.01% as mentioned in Table 5. So, it would be interesting to extend Table 5, by presenting both best and worst case scenarios.

Response: In the manuscript, Aeolus was assumed to be operated on best case scenario. As is illustrated in Fig. 6, Aeolus performs better using new parameters. It is very meaningful if we can assess the impact of instrument operational instrument on

the wind observation uncertainties combined with the operational Aeolus instrument. This is also a topic that I'm very interested in. I think it can be studied as the next topic when we could get access to Aeolus L0 measurement product.

8. line 118: "we focus on the simulation of the wind retrieved method on Rayleigh channel, and assume that the cross-talk effect between Mie channel and Rayleigh channel is negligible". Based on this assumption, you can remove mentioning over scattering ratio in section 3.1.

Response: Thanks for your kind mention. In the revision, we will remove related expressions.

9. Derivation of Eq. (7) in Appendix could have been done more simple, by substituting A=B in Eq.(3) => $\sigma_{R_{ATM}} = \sigma_A/(N_A * sqrt(2))$ Substituting Eq. (4) in Eq.(6) and setting A=B => $SNR_{Ray} = (N_A * sqrt(2))/\sigma_A$

Response: Thanks for your kind suggestion. the method would make the derivation much more simple which should also assumed that $N_{S,A} = N_{S,B}$. In revisions, we will simplify the derivation method according to your suggestions.

10. Figure 2. For the 15:00 and 12:00 UTC orbits, half the orbit is in full darkness (so no SBR contribution), the other half in full daylight (a large SBR contribution). How is this reflected in figure 2?

11. Also in Figure 3, I would expect bi-modal accuracy statistics with very good quality at the dark part of the orbit (no SBR) and low quality in the day-light part (high SBR). So, what is exactly displayed in Figure 3? Please present both statistics separately. In the caption of figure 3, mention that this is winds from the Rayleigh channel in clean air conditions.

Response: Here we will respond to the above two questions together.

The main topic of this manuscript is to discuss the impact of SBR on the wind observation accuracy of spaceborne DWLs on different orbits, and how much the laser energy

should be set to achieve required accuracy. Therefore, we put emphasis on the worst cases of SBR.

In Fig. 2 of the manuscript, the maximum SBR of each grid (the earth was divided into $1^\circ \times 1^\circ$ grids) was illustrated. Because the SBR is not much different at the same latitude as Fig. 2 of the manuscript shows, the SBR are averaged within 10° latitude. Then the 10° latitude averaged atmospheric conditions were obtained from Ozone Monitoring Instrument (OMI) database as mentioned in subsection 2.2 of the manuscript. Finally, the 10° latitude averaged uncertainties of wind observation on Rayleigh channel derived and show in Fig. 3 of the manuscript. Therefore, the Fig. 2 and Fig. 3 of the manuscript are the worst cases of SBR with maximum Rayleigh channel uncertainties as the reviewer 2 suggests. The detailed reasons were described as follows.

Fig. 3 and Fig .1 of the supplement illustrate that the determinant of SBR for Aeolus is SZA. As Fig. 3 shows, the values of SBR received by Aeolus will reach maximum and maximal values near summer and winter solstice. To derive the largest SBR, the time zones near summer and winter solstice were selected.

It is found that we only briefly described how to calculate the SBR for single off-nadir points in the manuscript as the last paragraph of section 2.2 of the manuscript shows, but didn't not describe how the global distributions of SBR were obtained. In the revision, we will add relevant descriptions. The details can also refer to subsection 3.1 of (Zhang et al., 2019), and was described briefly here. After we derived the SBR of each off-nadir point, earth is divided into $1^\circ \times 1^\circ$ grids. Each $1^\circ \times 1^\circ$ grid would include several off-nadir points, and the maximum TOA radiance in the grid was picked as the value of SBR in this grid. Finally we could derive the global distributions of SBR using the grids. And the global distributions of SBR during 15 days near summer and winter solstice are illustrated in Fig. 2 of the manuscript.

As is indicated in Fig. 8, the received SBR reach maximum value near summer solstice for Aeolus as a whole. For each grid of the earth, does the values of SBR reach

maximum values near summer and winter solstice? The distribution of SZAs of 5 grids within one-year range of the three orbits are illustrated in Fig. 9. Fig. 9 illustrates that the SZAs of off-nadir points in North Hemisphere reach maximum values near summer solstice, and the SZAes of off-nadir points in Sorth Hemisphere reach maximum values near summer solstice. However, for the off-nadir points near equator, the SBR reach minimal value. Consider from majority off-nadir points, the time zones near summer and winter solstice were taken as the worst cases.

Because we did not explain why we select the SBR near summer and winter solstice to analyse in this manuscript, it may cause confusion for readers. In the revision, we will add the related expressions.

References

HOLTSLAG, A., SVENSSON, G., BAAS, P., BASU, S., BEARE, B., BELJAARS, A., BOSVELD, F. C., CUXART, J., LINDVALL, J., STEENEVELD, G. J., TJERNSTROM, M. Van de WIEL, B. (2013), "STABLE ATMOSPHERIC BOUNDARY LAYERS AND DIURNAL CYCLES Challenges for Weather and Climate Models", BULLETIN OF THE AMERICAN METEOROLOGICAL SOCIETY, Vol. 94 No. 11, pp. 1691-1706.

NAEGELI, C., SJOBERG, B., SCHNEIDER, S., LEE, P., FARA, D., ADKINS, D. ANDREOLI, L. (2004) National Polar-orbiting Operational Environmental Satellite System (NPOESS) Potential Pre-planned Product Improvement (P3I) Status. AGU Fall Meeting.
REITEBUCH, O., HUBER, D. NIKOLAUS, I. (2018) ATBD: ADM-Aeolus Level 1B Product., ESA.

REITEBUCH, O., PAFFRATH, U. LEIKE, I. (2006) ATBD: ADM-Aeolus Level 1B Product., ESA.

ZHANG, C., SUN, X., ZHANG, R., ZHAO, S., LU, W., LIU, Y. FAN, Z. (2019), "Impact of solar background radiation on the accuracy of wind observations of spaceborne Doppler

wind lidars based on their orbits and optical parameters", Optics Express, Vol. 27 No. 12, pp. A936-A952.

ZHANG, D. L. ZHENG, W. Z. (2004), "Diurnal cycles of surface winds and temperatures as simulated by five boundary layer parameterizations", JOURNAL OF APPLIED METEOROLOGY, Vol. 43 No. 1, pp. 157-169.

1

Please also note the supplement to this comment:
https://amt.copernicus.org/preprints/amt-2020-202/amt-2020-202-AC1-supplement.zip

---

Interactive comment on Atmos. Meas. Tech. Discuss., doi:10.5194/amt-2020-202, 2020.

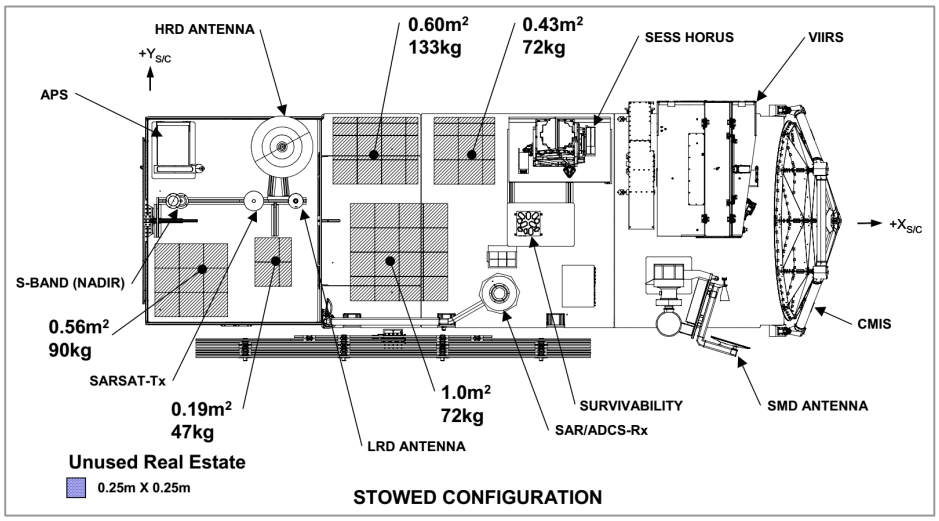

Fig. 1. Stowed configuration of NPOESS satellite operates on the orbit of 21:30 (Naegeli et al., 2004).

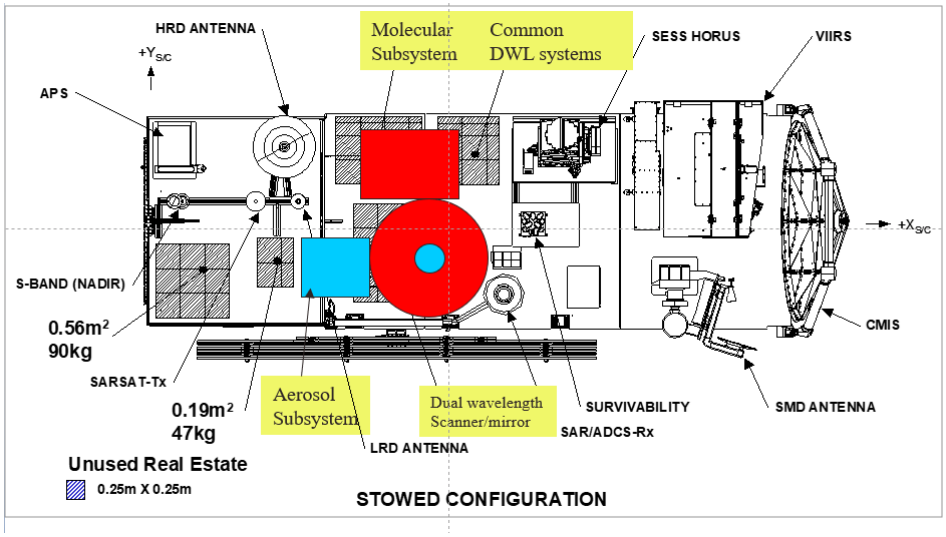

Fig. 2. The location of HDWL of NWOS in NPOESS satellite. (by DWL Mission Definition Team, 2005).

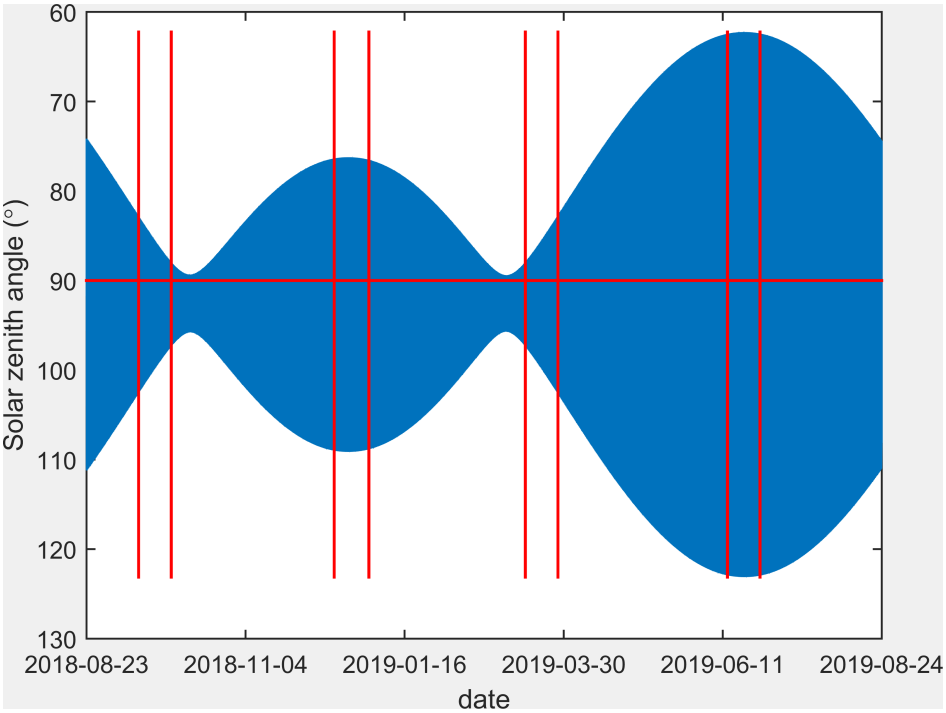

Fig. 3. The simulated solar zenith angle of the off-nadir points of Aeolus within one-year range.

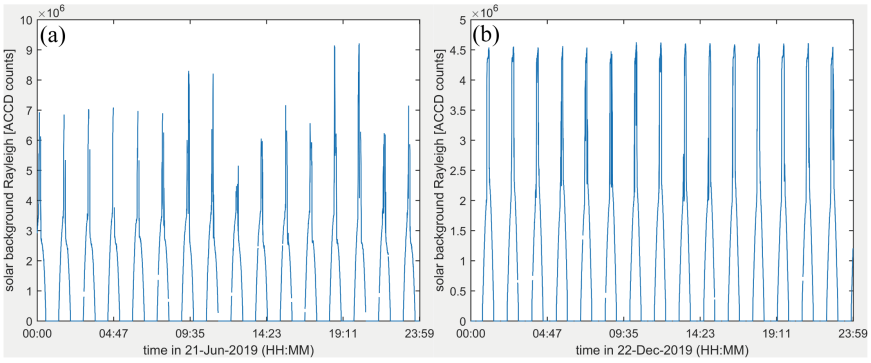

Fig. 4. The received solar background noise of Rayleigh channel (A+B) within 1 day. (a) summer solstice, (b) winter solstice.

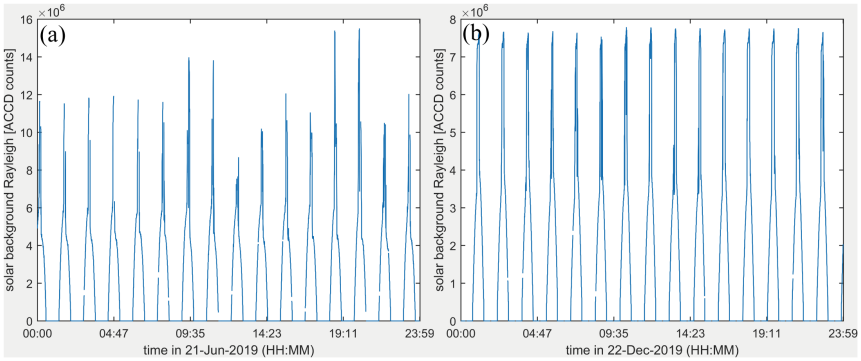

Fig. 5. Same as Fig. 4 using old instrument parameters shown in Tab. 1.

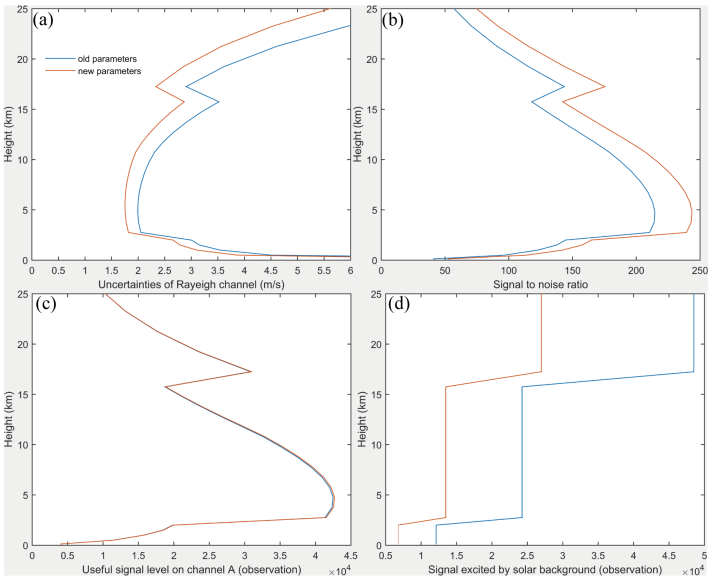

Fig. 6. Some simulation results obtained using old and new instrument parameters. (a)wind observations uncertainties; (b)Signal to noise ratio; (c)Useful signal; (d)Signal excited by SBN.

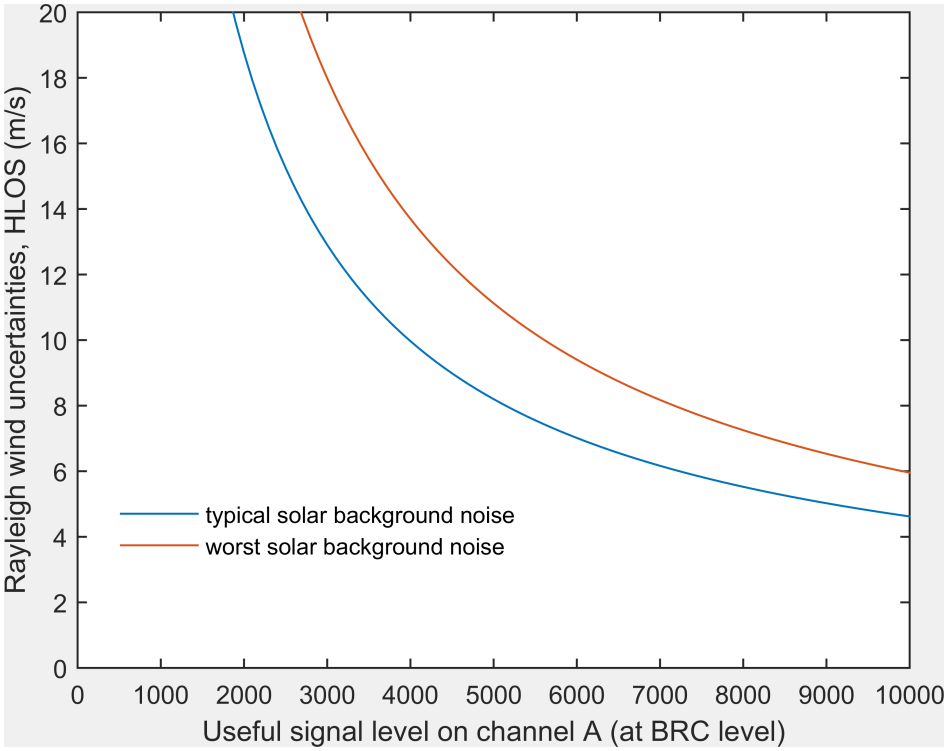

Fig. 7. The relationship between uncertainties of wind observations and useful signal of channel A on Rayleigh channel.

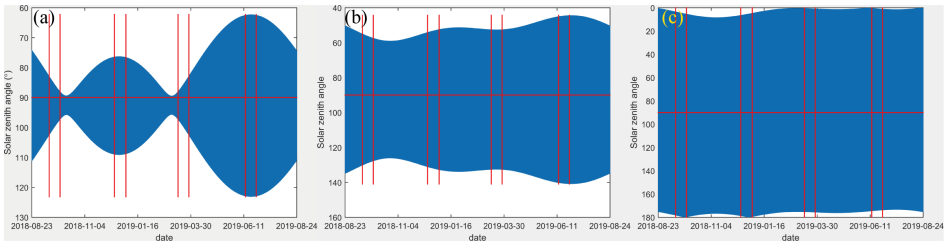

Fig. 8. The variations of SZA of the off-nadir points on the three orbits within one-year range. Sun-synchronous orbit with Local Time of Ascending Node crossing (LTAN) of 18:00 (a), 15:00(b) and 12:00(c).

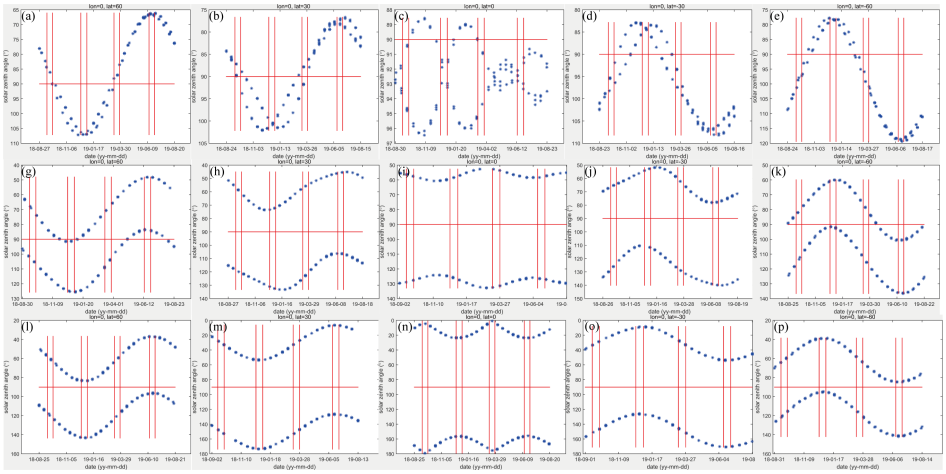

Fig. 9. Distributions of SZAs of 5 grids of three orbits within one-year range. Coordinates are (60°,0°), (30°,0°), (0°,0°), (-30°,0°), and (-60°,0°). Three rows are the 18:00, 15:00, and 12:00 UTC orbits.

Unit	Parameter	Symbol	Value	
			New	Old
ALADIN instrument	Number of measurements per observation	n_{meas}	30	14
	Number of pulses per measurement	n_{pulse}	20	50
	Optical transmission of instrument	$C(\lambda)$	0.34	0.8
	Field of View (FOV)	θ	18.1 μrad	22 μrad
	Diameter of telescope	D	1.5 m	1.5 m
	Vertical length of 25th range gate	Δz	200 km	200 km
	Bandwidth of the receiver	$\Delta\lambda$	1 nm	1 nm
	Wavelength of the receiver	λ	355 nm	355 nm
	Plank constant	h	$6.626*10^{-34}$	$6.626*10^{-34}$
	Light speed	c	$3*10^{8}$	$3*10^{8}$
Rayleigh Spectrometer	Fabry-Perot Free Spectral Range		4.56 pm	4.6 pm
	Peak transmission		81% / 67%	36.8%/27.2%
	Filter separation		2.33 pm	2.65 pm
	Filter FWHM (direct/reflected)		0.65pm/ 0.64 pm	0.74 pm / 0.70 pm
	Quantum efficiency		84%	75%

Fig. 10. Table 1. Main ALADIN instrument parameters.